

Electrodynamic ratchet motor

Jiufu Lim,^{1,*} John E. Sader,² and Paul Mulvaney¹

¹*School of Chemistry, The University of Melbourne, Victoria 3010, Australia*

²*Department of Mathematics and Statistics, The University of Melbourne, Victoria 3010, Australia*

(Received 11 November 2008; revised manuscript received 22 January 2009; published 27 March 2009)

Brownian ratchets produce directed motion through rectification of thermal fluctuations and have been used for separation processes and colloidal transport. We propose a flashing ratchet motor that enables the transduction of electrical energy into rotary micromechanical work. This is achieved through torque generation provided by boundary shaping of equipotential surfaces. The present device contrasts to previous implementations that focus on translational motion. Stochastic simulations elucidate the performance characteristics of this device as a function of its geometry. Miniaturization to nanoscale dimensions yields rotational speeds in excess of 1 kHz, which is comparable to biomolecular motors of similar size.

DOI: 10.1103/PhysRevE.79.030105

PACS number(s): 05.40.Jc, 87.85.Qr, 07.10.Cm

Miniaturization of devices to nanometer length scales greatly enhances the influence of thermal fluctuations. While this presents a fundamental limitation in some applications [1], it also facilitates the development of new devices that utilize Brownian motion in energy transduction [2]. One example that has received considerable attention in recent years is the flashing *on-off* ratchet [3]. These ratchets utilize asymmetric sawtooth-shaped potentials generated by barriers or external fields to partially rectify diffusive motion. Several implementations of on-off ratchets that provide translational motion and sorting capabilities have been presented [4–8]. The novel mechanism of Brownian motors is that their performance depends significantly on the diffusion of the particles or system [9]. Such a method is also believed to drive some biological motors [10]. Artificial molecular rotors have also been studied with reports of ratchetlike mechanisms [11]. These molecular rotors ultimately rely on charge distributions and conformational chemistry to form the ratchet potential landscape, and as such the nature of this energy landscape is largely speculative and is not open to direct measurement or manipulation.

In this Rapid Communication, we propose a design for a *rotary* flashing on-off Brownian ratchet that is amenable to modern microfabrication techniques. We take a fundamentally different approach by exploiting the geometry of equipotential surfaces. This achieves the necessary spatially varying potential to provide diffusion-induced rotary motion. To our knowledge, flashing ratchets have not been previously implemented for rotation. By utilizing rotary motion, our proposition presents a paradigm shift in the design and implementation of Brownian motors, which will find potential applications in energy conversion at the nanoscale. The scalability of our design facilitates tunability of the motor characteristics and thus implementation in practice. Unlike nanomechanical devices that are essentially miniaturizations of macroscopic three-phase motors [12], the electrodynamic ratchet motor we describe is designed to operate in a highly damped environment and takes advantage of the inherent Brownian motion at small length scales. The use of a single

stator also potentially improves durability and simplicity in practical operation.

This device is also in contrast to that of van den Broek and Van den Broeck [13], who recently proposed a chiral Brownian motor that requires two mechanically connected rotors to be isolated in two separate heat baths (at different temperatures). Complexity in implementation of such a device is circumvented in the present work since all components operate at the same temperature. This facilitates implementation using microelectromechanical system (MEMS) and nanoelectromechanical system (NEMS) technologies at length scales greater than molecular dimensions where Brownian motion is still prevalent.

Consider the cylindrical Brownian ratchet motor in Fig. 1. An outer stator comprises N_s teeth of asymmetric geometry, while the inner rotor has N_r teeth. Since both the stator and rotor are conductors, they admit electric potentials with an applied voltage of $\Delta V(t)$. As the rotor is constrained to rotate about the z axis, it will experience a torque, which would otherwise be absent if either the stator or rotor was perfectly circular.

An oscillating electrical potential $\Delta V(t) = V_0 \sin(2\pi\nu t)$ is applied to the motor to avoid undesirable electrolytic effects in the suspending medium. We consider the case where the frequency of oscillation is relatively small such that the electrostatic approximation holds for length scales below

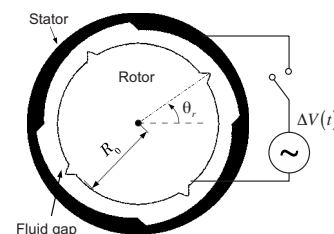


FIG. 1. Cross section of stator-rotor configuration with $N_s = N_r = 4$. Rotor protrusions are set to $0.1R_0$ in radial length and $0.1 \times 2\pi/N_r$ in angular span. The asymmetry factor of sawtoothlike stator boundary is $\alpha_s = 0.05$ ($\alpha_s = 0.5$ is symmetric) and the minimum radial gap between stator and rotor is $0.05R_0$. The potential difference between rotor and stator switches between $\Delta V(t) = V_0 \sin(2\pi\nu t)$ for on state and 0 for off state. θ_r is angular position.

*jiufulim@unimelb.edu.au

100 μm , yet much greater than the frequency of the fastest on-off cycling, i.e., $10 \text{ kHz} \ll \nu < 100 \text{ MHz}$. Effects due to the magnetic field components can then be ignored in the Maxwell stress tensor, i.e., $\vec{T} \approx \epsilon(\vec{E}\vec{E} - (1/2)E^2\vec{I})$. The resulting torque along the axis of the rotor, at a particular rotor position θ_r , is thus $\tau = (1/2)\epsilon(\nu)R_M^2L_z\int_0^{2\pi} E_r E_\theta d\theta$, assuming that the gap between the stator and rotor behaves as a linear medium with permittivity $\epsilon(\nu)$ under the applied field. The axial length of the rotor is denoted as L_z , whereas R_M is the radius of a cylinder enclosing the rotor that forms the integration surface. The inherent geometric asymmetry in the motor induces a torque; the integral of which gives the angular potential energy $U(\theta_r)$. This potential energy was calculated using the finite-element method within the electrostatic approximation: at each rotor position θ_r , the Laplace equation was solved numerically [14] within the gap between the rotor and the stator. The electric field components (E_r, E_θ) were readily obtained by finite differencing.

We introduce the following dimensionless parameters (denoted by the hat symbol): $\hat{r} = r/R_0$, $\hat{\nabla} = R_0\nabla$, $\hat{V} = \sqrt{\epsilon L_z/(2k_B T)}V$, and $\hat{\tau} = \tau/(k_B T)$, where R_0 is a characteristic radius of the rotary motor (see Fig. 1). The Laplace equation, torque τ , and corresponding potential-energy function U are then converted to dimensionless form as follows:

$$\hat{\nabla}^2 \hat{V} = 0, \quad (1a)$$

$$\hat{\tau}(\theta_r) = \frac{R_M}{R_0} \int_0^{2\pi} \left[\frac{\partial \hat{V}}{\partial \hat{r}} \frac{\partial \hat{V}}{\partial \theta} \right]_{r=R_M} d\theta, \quad (1b)$$

$$\hat{U}(\theta_r) = - \int_0^{\theta_r} \hat{\tau}(\theta'_r) d\theta'_r. \quad (1c)$$

The torque and potential energy increase with the square of the motor size. For the purpose of illustration, the following results assume the shape constants as depicted in Fig. 1. When there is a match in the periodicity of the stator and rotor, i.e., $N_s = N_r$, the periodicity of the resulting potential landscape is the same. In the case of a mismatch, a higher resultant periodicity is observed, which can be predicted using harmonic analysis. We approximate the rotor teeth as a ring of N_r test particles rigidly connected together with the regular spacing of $2\pi/N_r$. The stator is represented as a perfect sawtooth potential with a geometric asymmetry α_s that the rotor “particles” experience. It can be shown that the resulting number of periods in the potential N_p is given by

$$N_p = \frac{N_s N_r}{\text{gcf}(N_r, N_s)} = \text{lcm}(N_r, N_s), \quad (2)$$

where $\text{gcf} \equiv$ greatest common factor and $\text{lcm} \equiv$ lowest common multiple.

Merkle [15] also arrived at this result for rotational molecular bearings using number theory. However, Ref. [15] does not include an expression for the change in barrier height \hat{U}_0 (see Fig. 2). Using the harmonic theory above, this can be approximated as

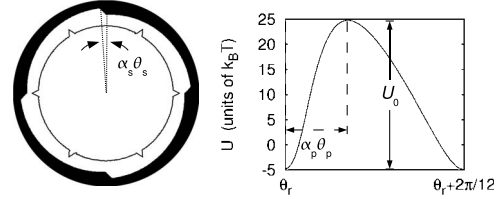


FIG. 2. Configuration with $N_s=4$, $N_r=6$ giving 12 effective periods. Sawtoothlike potential has asymmetry $\alpha_p=0.36$ calculated from relative position of the peak to the period θ_p . The geometric stator asymmetry is $\alpha_s=0.05$. $\hat{V}_0=8.5$ gives peak-to-peak height $U_0=30k_B T$. ($\theta_s=2\pi/N_s$ and $\theta_p=2\pi/N_p$).

$$\hat{U}_0 \sim \left(\frac{N_s}{N_p} \right)^2. \quad (3)$$

For example, a motor with $N_s=4$ and $N_r=6$ yields $N_p=12$ periods for the potential landscape using Eq. (2), although the barrier height \hat{U}_0 is reduced by 1 order of magnitude when compared to the matched case of $N_s=N_r=12$. This decrease in \hat{U}_0 can be readily compensated by increasing the applied voltage or immersing the motor in a medium of higher permittivity, enabling similar performance to be attained.

Consider the example motor in Fig. 2 with $N_s=4$, $N_r=6$, $R_0=10 \mu\text{m}$, and $L_z=10R_0$ operating in water at 25°C . To obtain a barrier height of $U_0=50k_B T$, an applied voltage of 3.7 mV is required when operating in ac mode. This is to be compared to the matched case of $N_s=N_r=12$, which requires 1.4 mV . Thus, through slight adjustment of the applied voltage, identical barrier heights are practically attainable.

To elucidate the performance of this motor for different stator-rotor configurations, with an applied external torque τ_{ext} , the system was simulated using the Fokker-Planck equation. We introduce the dimensionless time variable $\hat{t} = tk_B T / \gamma_r = tD_r$, where γ_r is the coefficient in the rotational Stokes' law $\tau = \gamma_r \omega$. With the aim of maximizing the mean angular velocity $\bar{\omega}$, the “off” duration of the applied voltage is chosen such that the rotor diffuses an angle $\alpha_p \theta_p$ in this time, i.e., $\hat{t}_{\text{off}} = (\alpha_p \theta_p)^2 / 2$, where α_p is the effective asymmetry of the resulting potential and $\theta_p = 2\pi/N_p$.

When the ratchet potential is switched on, the rotor must traverse the remaining period to admit net rotation. This (larger) angle then dictates the “on” time $\hat{t}_{\text{on}} = [(1 - \alpha_p)\theta_p]^2 / \hat{U}_0$. From this qualitative picture, an estimate for the average angular velocity can then be determined, $\bar{\omega} \sim N_p / \alpha_p^2$, which is valid in the high potential limit ($\hat{U}_0 \gg 1$) and strong asymmetry ($\alpha_p \ll 0.5$).

In the high-damping limit, where inertia is negligible, the Fokker-Planck equation can be used to describe the evolution of the system,

$$\frac{\partial \rho}{\partial \hat{t}} = - \frac{\partial}{\partial \theta_r} (\hat{D}_1 \rho) + \frac{\partial^2}{\partial \theta_r^2} (\hat{D}_2 \rho), \quad (4)$$

where $\rho(\theta_r, \hat{t})$ is the probability density of the rotor being at position θ_r at time \hat{t} . The drift \hat{D}_1 and diffusion \hat{D}_2 coefficients are given by

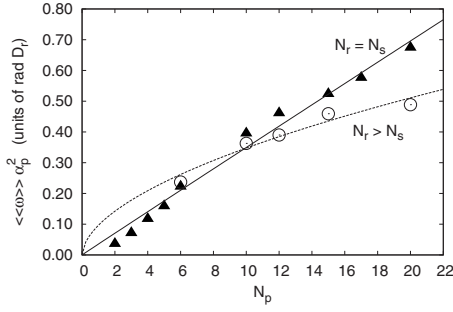


FIG. 3. For the same barrier height \hat{U}_0 (and neglecting changes in α_p), increasing the number of ratchet periods increases the average rotor speed. Solid triangles (▲) denote $N_r = N_s$ with a power-law fit $\bar{\omega}\alpha_p^2 = 0.036N_p^{0.99 \pm 0.064}$. The fit for the mismatched $N_r > N_s$ data (○) gave a nonlinear result $\bar{\omega}\alpha_p^2 = 0.097N_p^{0.56 \pm 0.080}$.

$$\hat{D}_1(\theta_r, \hat{t}) = \begin{cases} -\frac{\partial \hat{U}}{\partial \theta_r} - \hat{\tau}_{\text{ext}} & \text{(ratchet on)} \\ -\hat{\tau}_{\text{ext}} & \text{(ratchet off),} \end{cases} \quad (5a)$$

$$\hat{D}_2 = \hat{D}_r = 1. \quad (5b)$$

Equation (4) was solved using the path-integral method [16]. Initially, the dependence of the maximum rotor speed on the stator-rotor configuration was explored, i.e., without an applied external torque, $\tau_{\text{ext}} = 0$. The barrier height of each (N_s, N_r) configuration was normalized to $U_0 = 50k_B T$. For each configuration, an initial random distribution $\rho(\theta_r, 0) = 1/2\pi$ was evolved over 20 on-off cycles, $\hat{t}_{\text{cycle}} = \hat{t}_{\text{on}} + \hat{t}_{\text{off}}$. The first cycle was ignored in the subsequent analysis to minimize transients.

The time-averaged value $\bar{\omega}$ over this 19-cycle time interval was calculated using

$$\bar{\omega} \equiv \langle\langle \hat{\omega} \rangle\rangle_{\hat{t}} = \frac{1}{\hat{T}} \int_0^{\hat{T}} \int_0^{2\pi} \rho(\theta_r, \hat{t}) \hat{\omega}(\theta_r, \hat{t}) d\theta_r d\hat{t}, \quad (6)$$

where the instantaneous rotor speed was derived from the continuity equation $\hat{\omega}(\theta_r, \hat{t}) = \hat{D}_1 - (1/\rho) \partial \rho / \partial \theta_r$. From the above discussion, it follows that $\bar{\omega}\alpha_p^2$ should vary linearly with the effective periodicity N_p . This is verified by the data in Fig. 3 when the asymmetry is strong, i.e., $\alpha_p \ll 0.5$. However, for weak asymmetries, $\alpha_p \rightarrow 0.5$, directed diffusion is greatly reduced leading to violation of this scaling law. The fact that the potential walls (Fig. 2) are not perfectly linear and sawtooth in nature is another unaccounted detail in the derivation of this scaling. Table I illustrates that, in general, mismatches with $N_r > N_s$ give higher velocities than those with $N_r < N_s$. This is because cases where $N_r > N_s$ have slightly stronger asymmetry in the potential.

Although increasing the number of ratchet periods by employing a mismatched configuration can enhance the rotor speed, much of this improvement is offset by reduced asymmetry. The result is that speeds peak at an intermediate value of $N_p = 12$ for $N_r \neq N_s$. For example, the configuration

TABLE I. Averaged maximum rotor speeds of different stator-rotor combinations. Combinations with $N_{s,r} = 1$ were not evaluated (rows with dashes). $U_0 = 50k_B T$ and no external torque imposed.

N_p	$N_s = N_r$			$N_r < N_s$			$N_r > N_s$				
	α_p	$\bar{\omega}_{\text{max}}$		N_s	N_r	α_p	$\bar{\omega}_{\text{max}}$	N_s	N_r	α_p	$\bar{\omega}_{\text{max}}$
2	0.15	1.60									
3	0.18	2.20									
4	0.21	2.66									
5	0.23	3.00									
6	0.26	3.29	3	2	0.29	2.71	2	3	0.29	2.82	
10	0.32	3.86	5	2	0.38	2.52	2	5	0.36	2.80	
12	0.34	3.99	4	3	0.38	2.91	3	4	0.36	3.01	
15	0.36	5.67	5	3	0.40	2.77	3	5	0.40	2.87	
17	0.38	3.99									
20	0.38	4.67	5	4	0.42	2.90	4	5	0.42	2.77	

of $N_s = 3, N_r = 4$ yielding $N_p = 12$ provides a 13% improvement in maximum speed over the matched configuration ($N_s = N_r = 4$) for identical barrier heights.

Consider a microscopic ($N_s = 3, N_r = 4$) motor in water at 25 °C, with dimensions $R_0 = 10 \mu\text{m}$ and $L_z = 10R_0$. An applied voltage amplitude of $V_0 = 5.3 \text{ mV}$ is required to create a ratchet potential of $U_0 = 50k_B T$, resulting in a maximum speed of $\bar{\omega} = 1.0 \times 10^{-5} \text{ Hz}$. From the relation $\omega = D_r \hat{\omega}$, we find that the rotor speed scales as $\bar{\omega} \propto 1/(\mu R_0^3)$, where μ denotes the dynamic viscosity of the fluid. Consequently, if technological improvements allowed the fabrication of a 20-nm-radius motor, it could operate at 1300 Hz, comparable to sodium-driven bacterial flagellar motors of the same size [17].

Next, we examine the effect of applying an external torque. Motors of different (N_s, N_r) configurations were simulated up to a stopping torque $\tau_{\text{stop}} \approx \gamma_r \theta_p (1/2 - \alpha_p) / t_{\text{off}}$; this formula is derived for piecewise-linear sawtooth potentials [3]. Using the above analysis, this formula reduces to $\hat{\tau}_{\text{stop}} \approx N_p (1 - 2\alpha_p) / \alpha_p^2$. Power-law fits of the stopping torque data in Table II show qualitative agreement with this scaling law. The matched configurations resist the greatest torques due to their high potential asymmetry. For the example ($N_r = N_s = 4$) configuration above with a barrier height of $50k_B T$, a stopping torque of 37 pN nm is obtained.

For $U_0 \leq 50k_B T$, simulations yield a monotonically decreasing speed with increasing external torque. For much higher potentials, matched configurations with $N_p < 4$ give multivalued behavior where several values of torque produce identical motor speeds. The precise mechanism for this intriguing behavior is unclear but appears to arise from the ‘‘coarse’’ nature of low periodicity potential landscapes and the rotary geometry; this effect is eliminated as the periodicity is increased. Figure 4 is one example for a $N_s = N_r = 3$ configuration with $U_0 = 120k_B T$.

Finally, we assess the efficiency of this ratchet motor. The instantaneous power input is defined, $\hat{Q}_{\text{in}} \equiv \partial \hat{U} / \partial \hat{t}$, while the instantaneous work output is the product of the torque and the angular speed, i.e., $\hat{W}_{\text{out}} \equiv \hat{\tau}_{\text{ext}} \hat{\omega}$. The time averages for

TABLE II. Maximum values of input and output power and efficiency from intermediate values of the external torque. Mismatched combinations are italicized. $U_0=50k_B T$.

N_s	N_r	N_p	α_p	$\bar{Q}_{in,max}$	$\bar{W}_{out,max}$	$\bar{\eta}_{max}$	$\hat{\tau}_{stop}$
2	2	2	0.15	80	1.5	0.021	7.6
3	3	3	0.18	170	2.6	0.018	8.9
4	4	4	0.21	270	3.8	0.016	9.0
5	5	5	0.23	370	4.6	0.013	8.3
2	3	6	0.29	390	3.4	0.0093	5.4
6	6	6	0.26	480	5.0	0.011	7.4
2	5	10	0.36	830	2.7	0.0033	4.0
10	10	10	0.32	1100	5.7	0.0055	6.2
3	4	12	0.36	1200	3.2	0.0027	4.3
12	12	12	0.34	1400	5.7	0.0041	5.9
3	5	15	0.40	1600	2.6	0.0016	3.7
15	15	15	0.36	2000	5.6	0.0028	5.7
17	17	17	0.38	2400	5.2	0.0021	5.2
4	5	20	0.42	2600	2.4	9.2×10^{-4}	3.4
20	20	20	0.38	3400	6.9	0.0020	6.0

these quantities were calculated in the manner of Eq. (6) and the time-averaged efficiency given by $\bar{\eta} \equiv \bar{W}_{out} / \bar{Q}_{in}$. Each stator-rotor configuration was simulated as the torque τ_{ext} was increased. For each τ_{ext} , the average input or output power and efficiency were calculated. In all cases, the input power, output work, and efficiency reach a maximum for intermediate values of applied torque. These peak values are listed in Table II, showing decreasing maximum efficiency with increasing effective periodicity N_p . The matched configurations exhibit higher efficiency due to the stronger asymmetry in their potential.

We have presented an electrodynamic design for a Brownian ratchet rotary motor. This provides significant advantages over previous proposals that require different com-

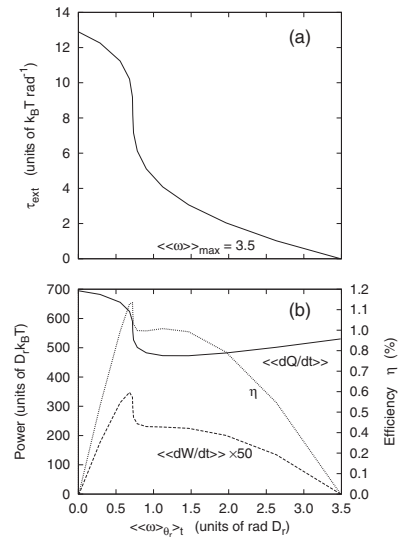


FIG. 4. (a) Torque-speed relationship at very high potential $U_0 = 120k_B T$ for $N_s=N_r=3$ shows multistable behavior where the average speed remains constant for $7 < \hat{\tau}_{ext} < 9$. (b) Peak power output and efficiency also occur at this range.

ponents of the motor to be immersed in isolated heat baths of different temperatures. Actuated rotation contrasts to previous works that have focused almost exclusively on translational motion. The scaling dependence of this motor was also elucidated, with the speed varying as the inverse cube of its radial size. This strong dependence allows for a dramatic enhancement in speed through miniaturization to the nano-scale; speeds comparable to protein motors are attainable. This simple design allows for great tunability in performance characteristics and implementation using MEMS and NEMS technologies over a wide range of length scales.

P.M. and J.E.S. acknowledge support from the Australian Research Council through the Discovery Grants Scheme. J.L. thanks the Albert Shimmins Fund for support.

- [1] F. J. Giessibl, Rev. Mod. Phys. **75**, 949 (2003).
 [2] P. Reimann, Phys. Rep. **361**, 57 (2002).
 [3] R. D. Astumian, Science **276**, 917 (1997).
 [4] J. Rousselet *et al.*, Nature (London) **370**, 446 (1994).
 [5] L. P. Faucheux, L. S. Bourdieu, P. D. Kaplan, and A. J. Libchaber, Phys. Rev. Lett. **74**, 1504 (1995).
 [6] L. Gorre-Talini, S. Jeanjean, and P. Silberzan, Phys. Rev. E **56**, 2025 (1997).
 [7] A. van Oudenaarden and S. G. Boxer, Science **285**, 1046 (1999).
 [8] J. S. Bader *et al.*, Proc. Natl. Acad. Sci. U.S.A. **96**, 13165 (1999).
 [9] P. Hänggi, F. Marchesoni, and F. Nori, Ann. Phys. (N.Y.) **14**, 51 (2005).
 [10] L. Mahadevan and P. Matsudaira, Science **288**, 95 (2000).
 [11] E. R. Kay *et al.*, Angew. Chem., Int. Ed. **46**, 72 (2007).
 [12] A. M. Fennimore *et al.*, Nature (London) **424**, 408 (2003).
 [13] M. van den Broek and C. Van den Broeck, Phys. Rev. Lett. **100**, 130601 (2008).
 [14] J. Burkardt, FFP_SPARSE: Finite element solution of Poisson's equation on a triangulated region, http://people.scs.fsu.edu/burkardt/cpp_src/ffp_sparse/ffp_sparse.html (2007).
 [15] R. C. Merkle, Nanotechnology **4**, 86 (1993).
 [16] H. Risken, *The Fokker-Planck Equation: Methods of Solution and Applications* (Springer-Verlag, New York, 1996).
 [17] G. Oster and H. Wang, Trends Cell Biol. **13**, 114 (2003).